water

MDPI

Article

Kinetics and Mechanistic Studies of Photochemical and Oxidative Stability of Galaxolide

Aneta Sokol *, Artur Ratkiewicz, Iwona Tomaszewska and Joanna Karpinska

Faculty of Chemistry, University of Bialystok, 15-245 Bialystok, Poland; artrat@uwb.edu.pl (A.R.); itomaszewska32@gmail.com (I.T.); joasia@uwb.edu.pl (J.K.)

* Correspondence: a.sokol@uwb.edu.pl

Abstract: Studies on kinetics of galaxolide (HHCB) degradation under influence of UV, simulated sunlight and some advanced oxidation processes (H_2O_2, UV/H_2O_2, and Vis/H_2O_2) were conducted. Galaxolide appeared to be a photolabile compound. The first-order kinetics model was assumed for all studied processes. It was observed that basic pH favored HHCB degradation. The influence of natural matrices (river water and artificial sweat) on direct photolysis of HHCB was examined. It was stated that the process of the photodegradation proceeded slower at the presence of each matrix. HHCB lactone was identified using the GC-MS technique. The recorded chromatograms showed that apart from the lactone, other degradation products were formed that we could not identify. In order to deeper understand the HHCB degradation process, DFT calculations were performed. The results pointed out that OH radicals play a key role in HHCB decomposition, which mainly proceeds via H abstractions as well as OH additions. It follows from the calculations that the visible light is sufficient to initiate the advanced oxidation processes (AOP_s) under the oxidative conditions, whereas UV irradiation is needed to start decay with no oxidative agents.

Keywords: galaxolide (HHCB); photodegradation processes; advanced oxidation processes; DFT study

Citation: Sokol, A.; Ratkiewicz, A.; Tomaszewska, I.; Karpinska, J. Kinetics and Mechanistic Studies of Photochemical and Oxidative Stability of Galaxolide. *Water* **2021**, *13*, 1813. https://doi.org/10.3390/w13131813

Academic Editor: Sergi Garcia-Segura

Received: 26 May 2021
Accepted: 28 June 2021
Published: 30 June 2021

1. Introduction

Galaxolide is a representative member of the synthetic polycyclic musks group of compounds. Its chemical formula is presented in Figure 1. Due to its low costs of production and nice clean sweet musky floral woody odor it has found a wide application as a fragrance ingredient in personal care products (PCPs) such as shampoos, lotions, soaps, deodorants, washing and cleaning products as well as in perfumes and cosmetics industries [1]. According to the available data of the European Union Risk Assessment Report, its annual production volume in Europe is between 1000 and 5000 tons year^{-1} (HHCB undiluted) [2]. Its content in consumer products varies from about 1000 to over 100,000 ng g^{-1} but the highest concentration of galaxolide occurs in perfumes—over 1,000,000 ng g^{-1} [1]. Due to such widespread use, it is found in every environmental compartment: surface waters [3–5], sediments [6,7], biota [8–10], air [11], sludge [4], and even in drinking water [12]. Because of its lipophilic nature (log K_{ow} = 5.90, its solubility in water equals 1.75 mg L^{-1} at 25 °C [13]) it exhibits affinity to fats and easily penetrates the food chain and tends to accumulate in living organisms' adipose tissues [6–10].

After using cosmetics or detergents, HHCB is transported with wastewater to wastewater treatment plants (WWTP) [14]. The detailed studies showed that it is liable to aerobic and anaerobic biotransformation [15] as well as to physical processes such as sorption onto active sludge [16]. Its removal efficiency is in the range of 30–99.7% and depends on the applied technology, the construction of the reactors and their numbers as well as the additional advanced oxidation modules used [15–18]. However, due to its widespread use and continuous supply to the treatment plants, it is perceived as a persistent pollutant [1]. Its concentration in the WWTP influent ranges from 1.9 to 16 µg L^{-1} [15–18] and in the effluent from 0.2 to 7.0 µg L^{-1} [12,15,16,18]. It is found in surface waters at the relatively

low level below 100 ng L^{-1} [5,12] while in drinking water detected at the trace level below 30 ng L^{-1} or below LOD of the applied analytical procedure [12]. However, taking into account its ubiquitous presence in every environmental compartment and continuous use, the ratio of the level of its major degradation product HHCB-lactone to the HHCB level is applied as an indicator of anthropogenic pressure on surface waters [14]. Although its concentration in surface waters is low, its presence is not neutral to organisms living in this environment. Several studies indicated that permanent exposition to a tiny concentration of HHCB induces oxidative stress in aqueous organisms [19–21]. It is proved that continuous exposure to its environmental concentrations albeit it has not caused acute toxicity [21], resulted in increased lipid peroxidation and protein carbonyl levels [20,21]. The 21 days exposition of *Dressena polymorpha* with the use of 100 and 500 ng HHCB L^{-1} solutions demonstrated its high potential to DNA strand breaks but has not caused any viable fixed genetic damage [20]. The provided results indicated that adverse effects of HHCB varied with organism species [22,23]. Because HHCB is present in almost every personal care product, humans are also heavily exposed to it, mainly through the skin. The total dermal daily exposure of adults to HHCB has been found to be 904 µg day^{-1} [24]. Taking into account the volatilization of HHCB only 78% of the amount applied on the skin penetrates the body [24]. There it is deposited mainly in the adipose tissues [25] but also is able to contaminate the human breast milk [26,27]. The daily intake of HHCB along with mother's milk by infants is assessed to be in the range from 40 to 180 ng kg^{-1} body weight [26,27]. Studies provided by Correia et al. [28] revealed that the dermal exposure of young children aged 0–5 years is quite low and amounts to 227.1 µg day^{-1}. Despite the relatively low amount to which young children are exposed, long-term health and developmental effects are difficult to predict. Some researchers hypothesize that one of the reasons for the increased frequency of autism spectrum disorders (ASD) is the exposure of the developing fetus to compounds contained in cosmetics and perfumes, including HHCB used by women during pregnancy [29]. Studies provided by Bagsra et al. [29] have proved that the majority of perfumes are mutagenic at femtomolar concentration and negatively affected human neuroblastoma cells. Considering the above facts, it seems that reducing the overall HHCB load in waters is still an ongoing task. For this purpose, many advanced oxidation processes (AOPs), as well as biological methods, were proposed. As HHCB underwent biotransformation some aqueous organisms such as algal [22] or fungi [23] were tested. Detailed studies have shown that the efficiency of HHCB removal by aqueous organisms differs significantly between species [22,23] and additionally depends on the design of wetlands [15]. The application of chemical and photochemical processes seems to give the best results. For this purpose, several AOPs includes direct irradiation by UV [30,31], ozonation [31–33], and photocatalysis [32,34] have been tested. The obtained results have pointed that among all processes tested the ozonation is characterized by the highest removal efficiency. The 30 min contact with 1.0 mg O_3 per mg DOC dose has caused almost 100% degradation of HHCB [33]. There is believed that the pivotal role in HHCB degradation is playing by hydroxyl radical [34,35]. The investigation of HHCB-OH radical reaction in the gas phase using density functional theory (DFT) has proved that it proceeds through two competing mechanisms: OH addition and hydrogen abstraction [36]. The degradation products were isolated and identified [34,35]. It was stated that under influence of the UV irradiation 5-isopropyl-1,1,2,3,3,6-hexametlylindanE, 3,5,5,6,7,7-hexamethyl-3,5,6,7-tetrahydro-2H-s-indacen-1-on, 6-isopropyl-1,1,2,3,3-pentamethyl-5-indancarbaldehyde were formed [30]. The photocatalytic degradation of HHCB with the use TiO_2 led to formation 1,3,4,6,7,8-hexahydro-4,6,6,7,8,8-hexamethylocyklopenta[γ]-2-hydroxybenzopirane, 1,3,4,6,7,8-hexahydro-4,6,6,7,8,8-pentamethyl-oxo-cyklopenta[γ]-phenol, 1,3,4,6,7,8-hexahydro-4,6,6,7,8,8-pentamethyl-oxo-cyklopenta[γ]-dihydroxybenzene, and 1,3,4,6,7,8-hexahydro-4,6,6,7,8,8-hexamethyl-cyclopenta[γ]-2-hydroxybenzopirane [34]. The presented data show that the advanced oxidation processes do not lead to complete mineralization of galaxolide but generate new compounds which the durability and the impact on living organisms are not fully

known [37]. So, the search for more effective purification processes leading to the complete removal of HHCB and not generating new chemical compounds is still an open problem.

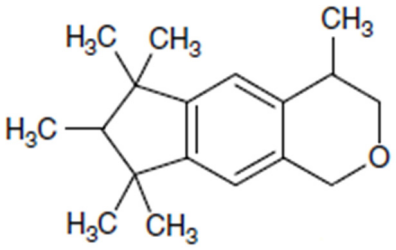

CAS 1222-05-5

Molecular weight 258.4

Log K_{ow} 5.9–6.3

K_{oc} 6300

Figure 1. Chemical structure of HHCB (1,3,4,6,7,8-hexahydro-4,6,6,7,8,8-hexamethylcyklopenta-gamma-2-benzopyran, trade name Galaxolide).

In the present work photolytic degradation of HHCB under influence of UV, simulated sunlight, H_2O_2, UV/H_2O_2, and Vis/H_2O_2 were investigated with the scope to studying kinetics and efficiency of HHCB dissipation at the presence of water MilliQ, river water or artificial sweat matrix. For this purpose, UV-Vis, spectrophotometry, and HPLC with fluorescence detection were applied. Another aim of this work was the identification of the main photoproducts HHCB generated from UV and Vis irradiation, Vis/H_2O_2, and UV/H_2O_2 treatments. Identification of HHCB photoproducts was carried out by GC/MS analysis.

A new aspect of this work is the comparison of the kinetics of HHCB decomposition under the influence of various factors such as UV and visible light, presence of oxidant and different matrices. The changes in HHCB concentration were monitored using simple spectrophotometric measurements and for the first time the newly proposed HPLC method with fluorescence detection (FLD). A novelty in the work is also a mechanistic study using the DFT approach. Theoretical research confirmed the results obtained by chromatographic methods.

2. Material and Methods

2.1. Chemicals

Galaxolide (Sigma-Aldrich, Steinheim am Albuch, Baden-Württemberg, Germany), a stock solution at the concentration 7.7×10^{-3} mol L^{-1} was prepared by dissolving an appropriate weight in 5 mL of ethanol and was stored in the dark at −4 °C. Working solutions at the concentrations 4×10^{-9}, 8×10^{-9}, 8×10^{-8}, 3.5×10^{-7}, 6×10^{-7}, 8×10^{-7}, 4.5×10^{-6}, 9×10^{-6}, 2.5×10^{-6}, 7.5×10^{-6}, 8×10^{-6} mol L^{-1} were prepared by dilution in MilliQ water. Hydrogen peroxide (POCH, Gliwice, Poland) at the concentration of 10^{-2}, 10^{-3}, 5×10^{-4} mol L^{-1} was prepared daily by suitable diluting of its 30% solution in MilliQ water. Acetonitrile and methanol of HPLC grade were supplied by Honeywell Chemicals. Other reagents used, supplied by POCh, Gliwice, Poland, were: concentrated ammonium (Sigma-Aldrich) and ethanol with purity higher than 96%, concentrated acetic acid, sodium hydroxide, and sulfuric acid solutions at the concentration 1 mol L^{-1}, sodium chloride.

2.2. Analytical Procedures

2.2.1. Absorbance (A) Measurements

Monitoring of the current concentration of HHCB was carried out spectrophotometrically by reading the absorbance at 226 nm. For qualitative assessment of changes in HHCB concentration, a calibration plot (ABS = $1.8 \times 10^4 \pm 1.5 \times 10^2$ (HHCB) + $3.2 \times 10^{-2} \pm 6.78 \times 10^{-3}$, $r^2 = 0.996$, where ABS—absorbance, (HHCB)—concentration of HHCB in mol L^{-1}) was constructed for concentrations in the range 10^{-6}–10^{-4} mol L^{-1}. The developed spectrophotometric method of HHCB determination was characterized by low LOQ and LOD values equal to 4.0×10^{-6} and 1.3×10^{-6} mol L^{-1}, respectively. All spectrophotometric measurements were conducted with a Hitachi U-2800A spectrophotometer

(Hitachi High-Technologies Europe GmbH (Mannheim Office), Mannheim, Germany). The following working settings of the device were used: scan speed 1200 nm·min^{-1} and spectral bandwidth 1.5 nm.

2.2.2. Chromatographic Analysis

The variation of HHCB concentration during experiments was assayed by high-pressure liquid chromatography with fluorescence detection, HPLC-FLD. The chromatographic separations followed by an FLD analyzer were run on C_{18} column Hypersil Gold (250 × 4.6 mm, 5 µm) using Thermo Scientific UltiMate 3000 HPLC instrument (Dionex, Sunnyvale, CA, USA). The HPLC system consisted of a pump, autosampler, column compartment, fluorescence detector (Thermo Scientific Dionex), and controlled by Thermo Scientific Dionex Chromeleon chromatography data system (CDS) software. Injection volume was 100 µL and flow rate 0.6 mL·min^{-1}. Gradient mobile phase composition was adopted: 50/50 to 90/10 in 35 min acetic acid 0.07% in acetonitrile/acetic acid 0.09% in water, then 3 min 90/10.2 min 90/10 to 50/50 and other 5 min 50/50. The excitation wavelength of the fluorescence detector was set to 280 nm. The emission wavelength of the fluorescence detector was set to 310 nm. The total run time was 40 min, and the HHCB peak showed a retention time of 27.97 min. An eleven-point and seven-point calibration curve was constructed by diluting the HHCB solution (10^{-2} mol L^{-1} in ethanol) in mobile phase (80:20 acetonitrile/water, acidified acetic acid) at concentrations ranging from 4×10^{-9} to 8×10^{-6} mol L^{-1}–HHCB (4×10^{-9}, 8×10^{-9}, 8×10^{-8}, 3.5×10^{-7}, 6×10^{-7}, 8×10^{-7}, 4.5×10^{-6}, 2.5×10^{-6}, 7.5×10^{-6}, 8×10^{-6}, 9×10^{-6} mol L^{-1}). The calibration curves were constructed by plotting the area against the HHCB concentration (n = 3).

Under the optimal detection conditions, the validation parameters of the developed FL method, such as linearity, the limit of detection, precision and repeatability, and others (Table 1), were determined. The detection limit (LOD) and limit of quantification (LOQ) of the investigated compound were counted according to the equations: LOD = 3.3 × s/a and LOQ = 10 × s/a (s—standard deviation, a—slop of the calibration curve). The precision of the method was evaluated by the analysis of four replicates of samples containing: 6×10^{-7}, 8×10^{-6} mol L^{-1} of HHCB. The reproducibility was obtained by preparing three independent calibration graphs on three different days resulted in an average slope of 8.18×10^{11}.

Table 1. Analytical data for determination of HHCB in HPLC with FLD detector.

Validation Parameter	Value/Equation
Linear range (mol L^{-1})	4×10^{-9}–9×10^{-6}
Slope	8.18×10^{11}
Intercept	41712
Correlation coefficient (r)	0.9996
LOD mol L^{-1}	3.63×10^{-10}
LOQ mol L^{-1}	1.10×10^{-9}
Precision (n = 4), R.S.D. %	2.08
Reproducibility R.S.D. %	0.68

The identification of the main products of photodecomposition of HHCB was performed by GC/MS technique. GC/MS analysis was carried out using an HP 6890 gas chromatograph with an electronic pressure control device connected to a mass spectrometric detector MSD 5973 (electron impact source and quadrupole analyzer, Agilent Technologies, Santa Clara, CA, USA) equipped with an HP-5MS column (5% phenyl, 95% methylsiloxane) with a length of 30 m and an i.d. of 0.25 mm coated with a 0.25 µm thick film and using a split/splitless injector. The injector worked in the splitless mode at a temperature of 250 °C. The helium of 99.999% purity was used as a carrier gas at a flow rate of 1.7 mL·min^{-1}. The temperature of the oven was programmed to 150 °C (1 min hold) and was increasing at a rate of 15 °C min^{-1} to 280 °C, maintaining finally the maximum temperature for

10 min. The total run time was 32 min. The MS detector worked under the following conditions: temperature of the ion source 230 °C, the temperature of the quadrupole 150 °C, the temperature of the transfer line 280 °C, mass range (m/z) 50–400.

2.3. Irradiation Procedures

All irradiation experiments were carried out using a UV lamp and solar light simulator.

UV-lamp standard 16AV, (Cobrabid, Poznan, Poland) equipped with two independent light sources emitting radiation at 254 and 336 nm was used. The UV irradiation experiments were performed using a 254 nm lamp. Solar light simulator (SUNTEST CPS+, ATLAS, Champaign, IL, USA) emitting radiation in the range of 300–800 nm was used for experiments in simulated natural conditions. The temperature in the simulator was maintained at 30 °C. To check the influence of Vis light intensity on the kinetics of HHCB degradation the lamp was working in two modes set at 375 or 750 Wm^{-2} for all photolysis experiments. All irradiation experiments were conducted in a crystallization dish with 100 mL capacity with the surface area open to the atmosphere.

2.3.1. Direct Photolysis

Two sets of experiments were performed: in the first one the HHCB laboratory solutions (without natural matrix) were subjected to irradiation according to the following procedure: 50 milliliters of working aqueous solution of HHCB at the concentration of 5.0×10^{-5} mol L^{-1} and pH 5.6 or 8.7 was subjected to the irradiation by solar light in a solar simulator chamber. The spectrum of the solution was recorded every 10 min. The pH of the aqueous solution was adjusted with 0.1 mol L^{-1} NaOH. A mixture of reagents (water and 0.1 mol L^{-1} NaOH) without HHCB irradiated at the same period was applied as a blank.

Dark control with solutions at the concentration HHCB 5.0×10^{-5} mol L^{-1} was performed to check the influence of temperature on the analytical signals of the analyte. The thermal dark tests were conducted by placing the HHCB solution in a glass test tube wrapped in aluminum foil to protect against light into the water bath at temperature 65 °C to study the thermal stability of galaxolide.

In the second set of experiments, the examination of photolysis in the environmental condition and physiological fluids was conducted using samples of surface water or artificial sweat as solvent. A total of 50 mL of working solution of HHCB (5×10^{-5} mol L^{-1}) with accompanied matrix was subjected to irradiation by solar light in a solar simulator chamber. The chromatograms of the solution were recorded every 10 min. Fresh surface water used in this study was collected from the local river. The taken samples were filtered through membrane with pore size 0.22 µm before use to remove suspended particles. Artificial sweat was formulated by the EN1811-1999 standard as reported by Kulthong et al. [38]. Briefly, the artificial sweat contained 5 g L^{-1} NaCl, 1 g L^{-1} urea, and 1 g L^{-1} lactic acid. The pH adjusted to 6.5 using ammonium solution was measured with an Elmetron CP-501 pH-meter (produced by ELMETRON, Zabrze, Poland) equipped with a pH-electrode EPS-1 (ELMETRON, Zabrze, Poland).

2.3.2. H_2O_2-Assisted Photodegradation Process

H_2O_2-assisted photodegradation was studied using a working aqueous solution of HHCB at the concentration 5×10^{-5} mol L^{-1}. For this purpose, an appropriate volume of HHCB aqueous solution (pH 5.8) was mixed with varying volumes of hydrogen peroxide to obtain the final concentration of the oxidant in the range 10^{-2}, 10^{-3}, 5×10^{-4} mol L^{-1}. The pH 8.7 of prepared mixtures was adjusted by adding a proper portion of NaOH solution at the concentration of 0.1 mol L^{-1}. Mixtures prepared in this way were thereafter subjected to irradiation by solar light in a solar simulator chamber or to the UV lamp (λ = 254 nm) for 80 min. The spectrum of the reaction solution was recorded every 10 min using the irradiated mixture of reagents without HHCB as a blank.

2.4. Separation of the Products of Photodecomposition of HHCB from an Aqueous Matrix

Because of the adverse effects that the aqueous matrix has for GC analysis, the conducted GC-MS analysis was followed by isolation (i.e., dispersive liquid–liquid microextraction-DLLME) of the studied compounds. The DLLME technique was chosen for this purpose because classical liquid–liquid extraction (LLE) or solid-phase extraction (SPE) procedures required the use of large organic solvents (5–10 mL) and sample volumes (surface waters: 2 to 1600 L), which resulted in longer analysis time and increased costs [39]. The applied procedure was as follows [40]: 5.00 mL of the aqueous solution was placed in a 10 mL glass tube with a conical bottom screw cap. Next, 620 µL of methanol (as dispersing solvent) containing 250 µL of chloroform (as extraction solvent) was quickly injected. After then the mixture was shaken gently until a cloudy solution was obtained and then it was centrifuged for 7.5 min at 4000 rpm. After centrifugation, the organic phase was separated from the aqueous phase and evaporated to a volume of 20 µL under a nitrogen atmosphere. The described DLLME procedure was applied for isolation compounds after direct photolysis and Vis/H_2O_2 and UV/H_2O_2 prior to GC-MS analysis.

2.5. Computational Methodology

All electronic structure calculations were performed at the temperature of 298.15 K and pressure of 1 atmosphere with the Gaussian 16 package [41], optimized structures were visualized with the Chemcraft program [42]. To model the environment (water) effect, the conductor-like polarizable continuum (CPCM) model was utilized [43], as implemented in the G16 program. To provide accurate description of the properties of the transition states and reactive intermediates the M06-2X functional, designed especially for chemical kinetics [44], was employed in conjunction with Dunning's correlation-consistent polarized valence basis set [3s2p1d/2s1p], denoted as cc-pVDZ [45]. This theory level was previously proven as a useful tool to capture the physical change along with the reaction coordinate for this type of reactions [46]. Normal mode analysis was performed to ensure the characteristics of the stationary points, i.e., the stable structure has zero imaginary ("negative") vibrational frequency, whereas the transition states (TS) have one and only one imaginary mode, corresponding to its reaction coordinate.

3. Results and Discussion

3.1. Kinetics of HHCB Direct Photolysis under Influence of Light

At the beginning of the performed experiments, a UV spectra of HHCB (5×10^{-5} mol L^{-1}) aqueous solution were recorded. Its spectral characteristics possessed three distinct maxima: sharp and intense at 196 with the shoulders at 226 nm, and broad and less intense at 280 nm (Figure 2). The photostability of aqueous solutions of HHCB was checked first. For this purpose, portions of 50 mL of its solution at concentration 5×10^{-5} mol L^{-1} were subjected to simulated solar light at intensity 750 and 350 W/m^2 irradiation. As measurements of absorbance at the chosen wavelength are fast and accurate, the changes in HHCB concentration were observed spectrophotometrically by monitoring the absorbance at 226 nm.

The primary experiments proved the photoliability of HHCB. There was observed a gradual decrease of the intensity of the absorbance band at 226 nm (Figure 2). According to available data [47,48], the first-order reaction model was assumed for studied processes. The obtained values of reaction constants, the corresponding half-live times of the HHCB and % of degradation after 80 min irradiation are listed in Table 2. It was observed that such factors as the kind of irradiation, intensity of irradiation, and pH of the reaction medium strongly influenced the rate of HHCB decomposition. It was stated that rates of the degradation of HHCB under influence of solar light ran from two and a half to three times faster than those of the UV-induced process (Table 2). The ongoing process of direct photolysis is more visible under the influence of radiation with an intensity of 750 W/m^2, k values of HHCB 3.5 10^{-3} min^{-1}. It was found that the alkaline pH favors the degradation of HHCB. As the temperature in the irradiation chamber of the solar

simulator is higher than room temperature (35 °C), the influence of temperature on HHCB stability was examined. The results obtained in the thermal dark test experiments (65 °C) demonstrated that no viable losses of analytes occurred by volatilization and/or thermal degradation [30]. It can be concluded that all observed changes in analytical response are due to the action of photons.

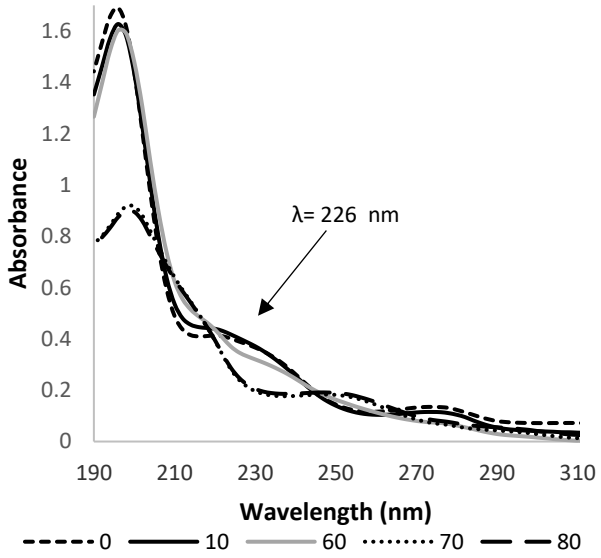

Figure 2. The changes in the UV spectrum of aqueous HHCB (5×10^{-5} mol L^{-1}), solution subjected to irradiation by simulated solar light at pH 5.8 versus MilliQ water as a blank. Spectra were recorded at different times of the process and thus 0, 10, 60, 70, 80 represent the observation time in minutes.

Table 2. First-order reaction constants, the corresponding half-live times and % degradation of the HHCB, direct photolysis, Vis/H_2O_2, and UV/H_2O_2, irradiation time–80 min.

Studied Process	pH	The Concentration of H_2O_2 mol L^{-1}	Molar Ratio H_2O_2/HHCB	k $min^{-1} \times 10^{-3}$	$t_{1/2}$ min	% of Degradation after 80 min
Irradiation time: 80 min						
Vis (E 750 W/m^2)	5.8	-	-	3.5	198	21.3
	8.7	-	-	4.3	161	25.9
Vis (E 375 W/m^2)	5.8	-	-	3.45	201	23.6
UV	5.8	-	-	1.3	533	12.1
	8.7	-	-	1.4	495	12.2
Vis/H_2O_2 (E 750 W/m^2)	5.8	10^{-3}	20	3.7	187	21.4
		10^{-2}	200	3.7	187	22.3
	8.7	10^{-2}	200	2.9	239	18.4
		10^{-3}	20	6.2	112	68.0
		5×10^{-4}	10	4.7	147	28.6
UV/H_2O_2	5.8	10^{-3}	20	2.1	330	19.1
		10^{-2}	200	1.9	365	11.8
	8.7	10^{-3}	20	4.4	157.5	31.4
		10^{-2}	200	17.3	40	87.0

3.2. Kinetics of HHCB Decomposition under Influence of UV/H_2O_2

The decomposition of HHCB in water under influence of the UV/H_2O_2 process was investigated next. The primary experiments proved that HHCB cannot be effectively removed by UV radiation and H_2O_2 oxidation alone, while UV/H_2O_2 assisted process appeared to be more effective and could degrade HHCB faster. The H_2O_2/UV advanced oxidation process is based on the photolysis reaction of the H_2O_2 (hydrogen peroxide) molecule and is favored by the basic pH. Hydroxyl radicals are formed during the decomposition of hydrogen peroxide and cause the degradation of organic pollutants. As the result, they are used in water technologies, e.g., wastewater or drinking water treatment. It was observed that the effectiveness of HHCB removal depends on the intensity and kind of light used, the concentration of oxidant, and pH (Table 2). The influence of H_2O_2 concentration was examined using its varying concentration in the range 5×10^{-4}–10^{-2} mol L^{-1} at two pH values pH (5.8 and 8.7). It was found that the HHCB degradation process meets the 1st order reaction model. When 20-fold excess of the oxidant concentration in ratio to galaxolide was applied, 31% increase was observed in the degradation rate in an alkaline environment and only 5% in an acidic environment, compared to the direct photolysis process. It was stated that increasing the concentration above this excess only slightly increases the rate of reaction (Figure 3).

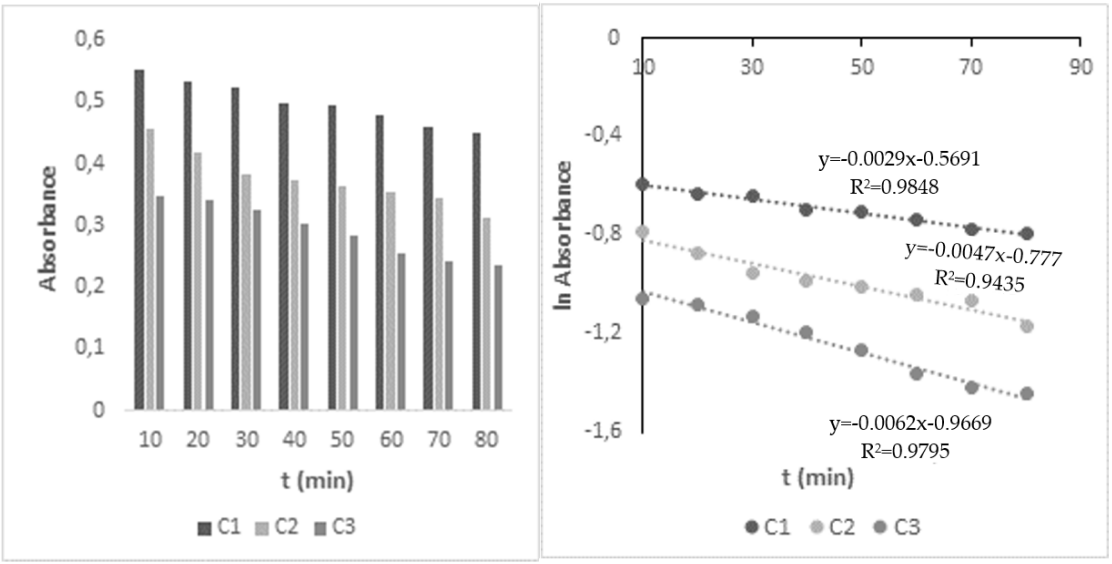

Figure 3. Changes in HHCB A(t) and lnA (t) under influence of Vis/H_2O_2 system, concentration of H_2O_2: C_1—10^{-2}, C_2—5×10^{-4}, C_3—10^{-3} mol L^{-1}, pH 8.7, irradiation time: 80 min.

The observed acceleration in the rate of HHCB disappearance can be explained as a result of combining two simultaneous processes. On the one hand, simulated sunlight triggers the direct photolysis of HHCB. At the same time, radiation breaks down hydrogen peroxide into hydroxyl radicals which react with HHCB. UV/H_2O_2 degradation of HHCB in the alkaline environment proceeds six-times faster than under UV alone, while in an acidic medium is only twice faster. UV radiation and a 200-fold excess of oxidant in the alkaline environment increase the rate of HHCB decomposition by 83%.

3.3. Photolysis of HHCB in Environmental Condition

The stability of HHCB under simulated environmental conditions was checked next. The goal of this experiment was to answer what is the persistence of this compound in natural conditions and what products are created. Because the selectivity and sensitivity of the spectrophotometric technique are not enough for this purpose, the HPLC-FLD procedure was used for monitoring the changes in analyte concentration. As the chemical composition of natural surface waters is very complex and difficult for reconstruction, real

samples of water taken from the local river were used as solvents for preparing working solutions of HHCB. Working solutions of HHCB were prepared according to the procedure in Section 2.1 using a sample of real water or artificial sweat as a solvent at the concentration 5×10^{-5} mol L^{-1} and next were subjected to irradiation in a sunlight simulator chamber. Every 10 min 2 mL of irradiated solution was taken and subjected to HPLC-FL analysis according to the procedure given in Section 2.2.2. HHCB retention time was 27.97 min. The degradation processes were tested in triplicate. Using the previously prepared standard curve for galaxolide, its temporary concentration was calculated. Assuming the first-order kinetics model of the degradation reaction, the kinetic parameters of the photodegradation reaction were determined (Table 3). The obtained results pointed that rates of the degradation of HHCB MilliQ solutions under influence of solar light ran 1.4- to 1.6-times faster than the photolysis process of HHCB in river water or the presence of artificial sweat (Table 3). The decomposition of HHCB occurs as a result of direct photolysis alone. The rate of its decomposition in the presence of such complex matrixes decreased due to competition for light access. The observed rate of the degradation of HHCB was at least 1.5-times lower than this for laboratory solutions. Although the % of degradation is the same after 120 min, matrix effects can be observed in the reaction time from 0 to 40 min (Table 3).

Table 3. The kinetics parameters of HHCB photodegradation in laboratory solutions and in the presence of surface water and artificial sweat matrix.

Studied Process	Used Irradiation	k (min^{-1}) $\times 10^{-2}$	$t_{1/2}$ (min)	% of Degradation after	
				40 min	120 min
Direct photolysis of laboratory solution	Vis (E 750 W/m^2)	4.93	14	93.6	99.9
	UV	2.92	24	58.9	99.8
Direct photolysis in presence of surface water matrix	Vis (E750 W/m^2)	3.57	19	74.5	98.9
Direct photolysis in presence of artificial sweat matrix		3.16	22	91.9	97.6

3.4. Identification of Transformation Photoproducts of HHCB

The aim of this work was the identification of photoproducts HHCB (TP) generated by UV and Vis irradiation and Vis/H_2O_2, and UV/H_2O_2 processes. The research was carried out using irradiated model solutions and at the presence of river water and artificial sweat. For this purpose, MilliQ HHCB solutions with a concentration of 5×10^{-5} mol L^{-1} and pH 5.6 and 8.7 were exposed to simulated UV radiation and sunlight and were also subjected to the processes taking place in the systems: Vis/H_2O_2 and UV/H_2O_2. After the fixed time of reaction, the resulted solutions were subjected to DLLE in order to isolate the residue of the parent compound and its degradation products. The analysis was performed by GC/MS technique.

It was observed that the concentration of generated photoproducts and their parent compounds in the irradiated solutions was too low for direct analysis by the GC-MS system. Additionally, the presence of an aqueous matrix was a setback. That is why, to carry out isolation and preconcentration of the analytes, DLLE extraction was employed. Examples of recorded GC-MS chromatograms are shown in Figure S1. It can be seen that after 100 min of irradiation the peak derived from HHCB (tR 13.44 min) completely disappeared but four new peaks of possibly forming photodegradation products appear (Table 4). The main HHCB transformation product (TP) HHCB-lactone (1,3,4,6,7,8-hexahydro-4,6,6,7,8,8-hexamethyl-cyclopenta [γ]-2-benzopyran; HHCB-lactone) was identified at retention time 16.60 min. HHCB-lactone is the most stable intermediate generated and it is frequently detected in river waters and wastewater [35]. Figure S2 shows the mass spectra of the obtained HHCB photodegradation products. The transformation of HHCB to HHCB-lactone has been investigated in several studies that have elucidated the different degradation steps [49]. Initially, HHCB is activated through the formation of hydroxyl radicals which is

followed by the addition of molecular oxygen. Peroxide moieties of the molecule are then formed which is followed by protonation and removal of a water molecule. The GC-MS analysis carried out indicates that under the influence of light, as well as other studied processes, several stable intermediate products are formed, but their identification due to the lack of spectra in databases, their exact identity has not been established. It is also possible that HHCB-lactone is hydroxylated to form the corresponding hydroxy acids, but these remain to be unidentified. The implication is that galaxolide lactone may be a relatively stable end-product [50].

Table 4. Identification of photoproducts generated by photolysis of HHCB investigated.

Name	Structure	Retention Index (I_R)	Retention Time (t_r min)	Quantification Ion (*m*/*z*, %)	Identification Ions (*m*/*z*, %)
HHCB	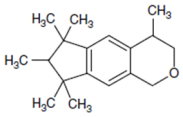	1872	13.44	243 (100)	258 (30), 213 (36)
HHCB-lactone main peak	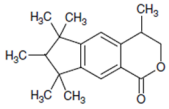	2206	16.60	257 (100)	272 (14), 197 (12)
HHCB-lactone secondary peak	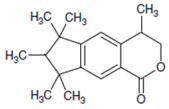	2247	16.95	257 (100)	272 (14), 197 (12)
Product transformation	NN–unidentified compound	2161	16.20	243 (100)	-
Product transformation	NN–unidentified compound	2287	17.20	273 (100)	-

3.5. A DFT Mechanistic Study of the Galaxolide Decay

As mentioned in the Introduction, a significant experimental interest in studying the degradation of galaxolide in a water environment is noted. Facing many technological challenges, experimental techniques to detect what occurs during a reaction curse are still in their infancy, however. Thus, to gain a deeper insight into the formation of products generated under both oxidative and irradiation conditions, quantitative density functional theory (DFT) calculations were conducted. The computed geometry parameters and harmonic frequencies of all the species considered in this section are available in the Supplementary Materials.

The photoinduced degradation of galaxolide was investigated experimentally in the ref [30]. Three major products were detected, namely 5-isopropyl-1,1,2,3,3,6-hexamethylindane, 3,5,5,6,7,7-hexamethyl-3,5,6,7-tetrahydro-2H-s-indacen-1-one and 6-isopropyl-1,1,2,3,3-pentamethyl-5-indancarbaldehyde, abbreviated as G1, G2 and G3, respectively. The reaction schemes leading to these products are proposed below, see Figure 4 (free energy profile) and Figure 5 (optimized geometries). It is noted, that all the free energy profiles reported here (Figures 4 and 6) were prepared with corrections taking into account species gained/lost during the particular steps, for the sake of clarity these corrections are not explicitly listed. For the same reason, in Figure 5 (and also in similar Figure 7, Figures S50 and S52) the H atoms are plotted only where omitting them may lead to misunderstanding, which is especially a case for the H atom metatheses. The multistep process starts with photoinduced cleavage of the bond connecting O and C atoms (bond 1-18, see Figure 5) in the heterocyclic ring. The barrier associated with this process is relatively high (~94 kcal/mol), which corresponds to ~305 nm (near UVB radiation spectrum). As it is seen from Figure 5, the initial ring breakage may lead to two different products. One of them is stable enough

to be detected by mass spectrometry (P1-G3 in ref. [30]), whereas the second one differs by H atom location, bonded to the C17 atom instead of C18, which makes it a highly unstable biradical intermediate (IM1) with significantly higher (>80 kcal/mol) energy. Its neutralization goes through two consecutive metatheses (H transfer from H_2O to galaxolide). This may occur in two ways, namely H transfer to C18(TS2A_v1→IM2A_v1) followed by H transfer to O (IM2A_v1→TS3A_v1→P3A), or TS2A_v2→IM2A_v2 →TS3A_v2→P3A. Both channels join at the stable (alcohol) product P3, which is transformed to stable product P5 (G1) via OH departure (TS4, P4) followed by H elimination via metathesis reaction with water molecule TS5→P5 (G1). G3 can also recyclize into a 5-membered ketone ring. This route starts from photolysis of the C17-H bond (TS2→P2), followed by the ring closure with the creation of the cyclic alcohol (P2→TS3→P3). P3 is, by the H elimination by H_2O molecule, further transferred to P4 (G2) cyclic ketone.

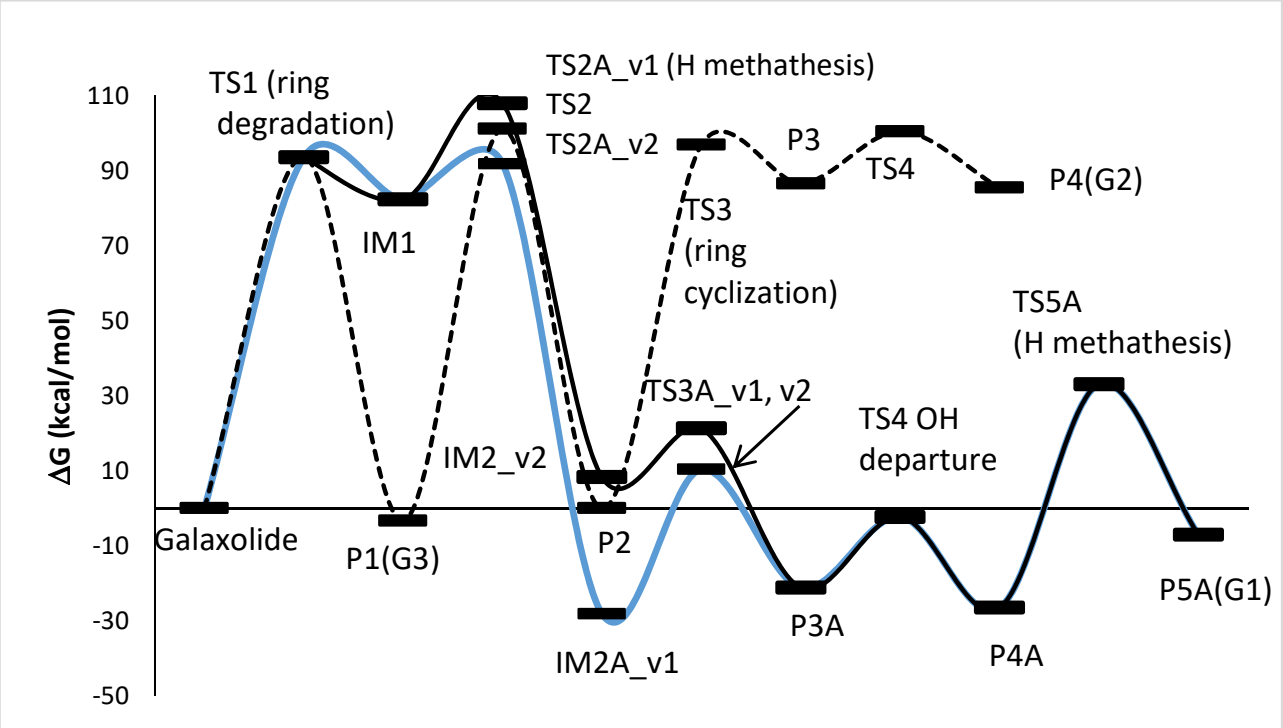

Figure 4. Energy profile of the proposed reaction mechanism under UV irradiation conditions. (in terms of ΔG values, kcal/mol). To be comparable with galaxolide, ΔG values were corrected with the values appropriate for species gained/lost during the reaction. Species are pictured in Figure 5.

It is known from experimental reports [34,35], that the mechanism of galaxolide decomposition under the oxidative conditions is far more complicated than the one detailed above, where UVB light caused ring breakings, followed by a series of the H additions/abstractions in the metatheses processes. The main oxidative agents are the hydroxyl radicals, formed during the decomposition of hydrogen peroxide. Because of their presence, energetic barriers of initialization are expected to be far smaller than these computed for the irradiation conditions. Since the OH additions are more likely to occur, the chemistry also becomes richer. Eighteen main intermediates were detected in Reference [35] (oxidative and/or irradiation conditions), compared to 3 from Reference [30] (UV irradiation). These 18 species can be classified according to these total ion current (TIC) peak intensities. To better understand the process, selected routes leading to the chemical individuals with the highest intensities were investigated in detail. For the product with the largest intensity (#17 in Reference [35], $C_{18}H_{24}O_2^+$ (ionic part, i.e., without the H^+, theoretical mass ~272 Da, called Product A hereafter), the reaction starts from H abstraction from C17 by OH radical. The associated barrier is about 7 kcal/mol, which is a very small value, compared to the

one needed to start the photochemical decomposition (>90 kcal/mol). The next step is OH addition to the same C atom (P1B→TS2B→P2B). Then, two H atoms need to be removed from the C17 and hydroxyl radical just added. This may be achieved by two subsequent H metatheses from reactant to OH radicals, the sequence of which makes two alternative pathways v1 and v2. The overall scheme is pictured in Figure 6, species are detailed in Figure 7. It is interesting to note, that whereas the barrier for the reaction initialization is small, much larger energies of almost 60 kcal/mol are needed for some subsequent steps. Under room temperature, such energies are provided by external irradiation, which seems to be necessary for the reaction to occur. Indeed, according to Reference [35], this channel was detected after UV, ozone, and Xe/Cat treatment. Hoverer, since 60 kcal/mol corresponds to ~480 nm, our calculations show that visible light (sunlight) should be sufficient for this route to proceed. The next path considered here (2-nd tic peak intensity in [35]) is pictured in Figure S50 (energy diagram) and Figure S51 (species explanation) in the Supplementary Materials. It starts from H abstraction from C18 or C16, which also produces two different, yet energetically similar, reaction channels. The subsequent H abstraction (both by metathesis with OH radical) results in double bond creation. In contrast to the previous one, this route is not energetically expensive, thus it is expected that it may take place even without irradiation. Additionally, the channel leading to the ionic part of the species #16 in Reference [35] ($C_{18}H_{24}O_2$, theoretical mass ~272 Da) starts from H abstraction from C18 with OH addition to the same C atom. Then, two different channels are possible, according to the sequence of the subsequent H metatheses, possible sequences are C16, O, and inversely. The created biradical immediately turns to cyclic ketone product C. The energy scheme and species plot for this channel are pictured in Figures S52 and S53 in the Supplementary Materials file.

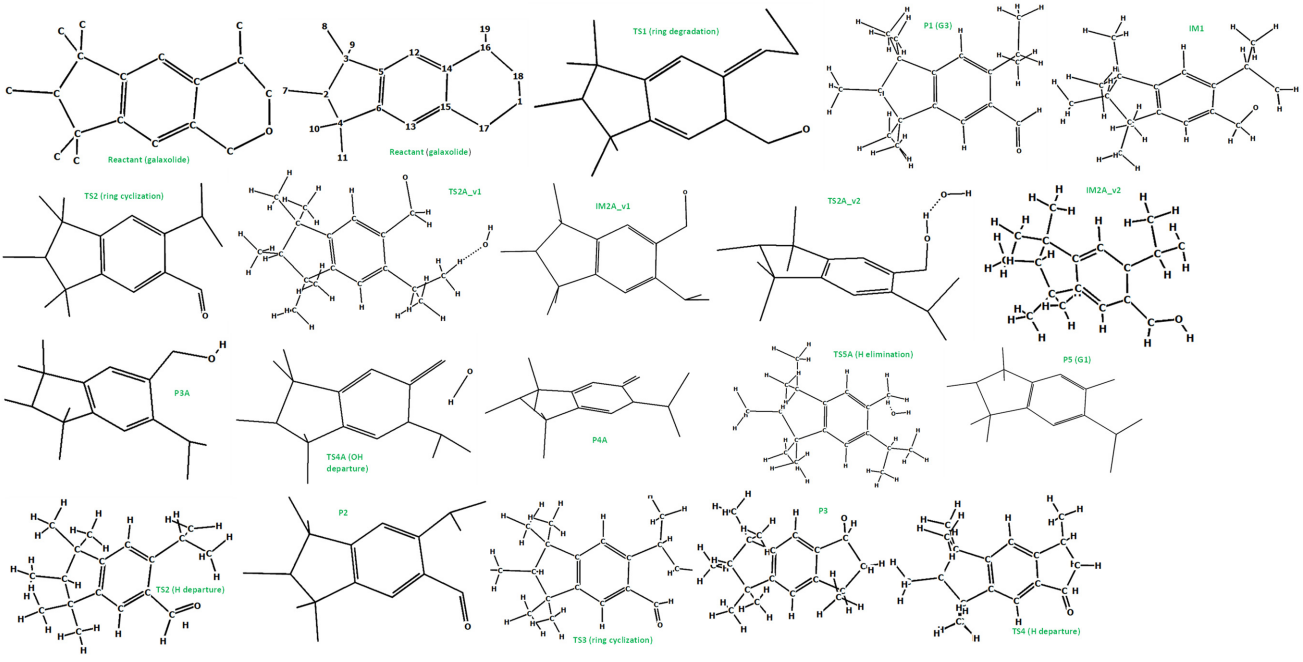

Figure 5. The optimized (at the M06-2X/cc-pVDZ level) geometries of the species involved in the reaction scheme from Figure 4.

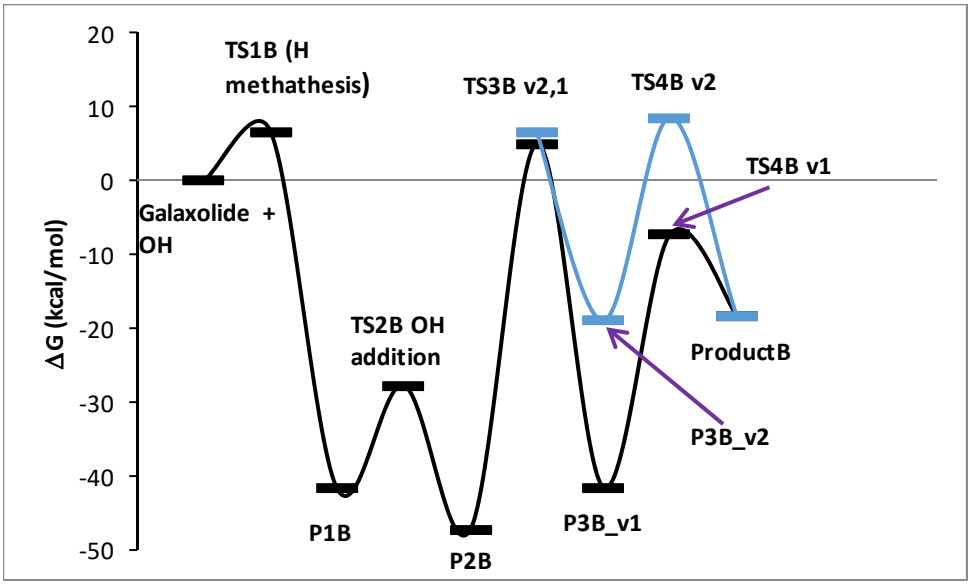

Figure 6. Energy profile of the proposed reaction mechanism under oxidative conditions (in terms of ΔG values, kcal/mol). To be comparable with galaxolide + OH, ΔG values were corrected with the values appropriate for species gained/lost during the reaction. Species are pictured in Figure 7.

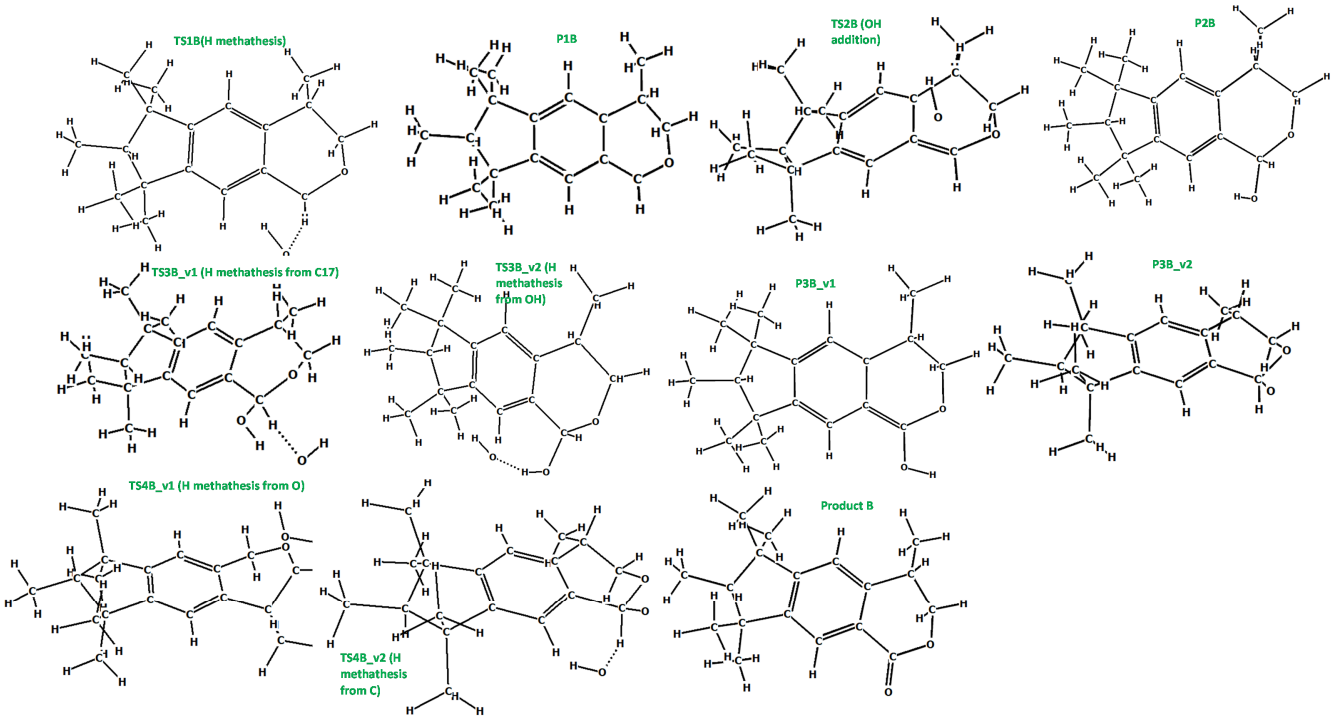

Figure 7. The optimized (at the M06-2X/cc-pVDZ level) geometries of the species involved in the reaction scheme from Figure 6.

4. Conclusions

The obtained results indicate that HHCB is a photolabile compound. The conducted experiments have shown that direct HHCB photolysis in model solutions occurs most quickly in an alkaline environment and under the influence of simulated sunlight. It was stated that the observed disappearance of HHCB in the model solutions was the result of direct photolysis. The presence of a natural matrix slightly reduces the degradation process. The course of HHCB degradation under the influence of hydroxyl radicals in the UV/H_2O_2

and Vis/H_2O_2 systems was also investigated. It was observed that the addition of an oxidant significantly accelerates the rate of HHCB degradation. As in the case of model solutions, the H_2O_2 assisted UV or Vis-photolysis is promoted by the alkaline environment. In an alkaline medium, UV radiation increases six times the rate of HHCB degradation in the presence of an oxidant compared to simulated sunlight. Sunlight is able to generate a sufficient amount of hydroxyl radicals resulting from the photolysis of hydrogen dioxide. The main degradation products were identified by the GC-MS technique. It was found that the main product of galaxolide degradation is its lactone, regardless of the process used (UV or Vis light or Vis/H_2O_2 and UV/H_2O_2 treatments, or in the presence of natural matrices). The DFT calculations provided a deeper insight into the mechanism of the photodegradation as well as the occurrence in an oxidative alkaline environment. The calculations suggest, that OH radicals play a crucial role in both environments. Near UVB light (or more energetic) need to be used to start the decomposition, which starts from the breakage of the heteroring. This process would not be possible without UVB irradiation. In the alkaline environment, the decay also begins from H abstractions by OH radicals, but OH additions to the ring/methyl substituents are also important. The energy provided by the sunlight is sufficient to obtain main products under such conditions, no UV irradiation is necessary. Musk metabolites are mostly the result of biotic or abiotic degradation of the parent compound, both in wastewater treatment plants in water and sediments of receiving surfaces and in organisms.

Supplementary Materials: The following are available online at https://www.mdpi.com/article/10.3390/w13131813/s1. Tables of optimized geometries and harmonic frequencies, calculated at the CPCM/M06-2X/cc-pVDZ level of theory for all the species considered. Energetics schemes and species plots of the reactions channels leading to Product C and product D.

Author Contributions: Conceptualization, A.S. and J.K.; methodology A.S. and J.K.; DFT study, A.R.; investigation, I.T. and A.S.; writing, A.S., J.K. and A.R.; writing—review and editing, A.S. and J.K.; visualization, A.S. and A.R.; supervision, A.S. All authors have read and agreed to the published version of the manuscript.

Funding: The work was partially financed by EU founds via project with contract number POPW.01.03.00-20-034/09-00, POPW.01.03.00-20-004/11-00, COST Action MP1302 Nanospectroscopy, and by NSC–Poland founds, project number 2014/13/N/ST5/00568.

Institutional Review Board Statement: Not applicable.

Informed Consent Statement: Not applicable.

Data Availability Statement: Not applicable.

Acknowledgments: The authors would like to thank the Computational Center of the University of Bialystok (Grant GO-008) for providing access to the supercomputer resources and the GAUSSIAN 16 program.

Conflicts of Interest: The authors declare no conflict of interest.

References

1. Reiner, J.L.; Kannan, K. A survey of polycyclic musks in selected household commodities from the United States. *Chemosphere* **2005**, *62*, 867–873. [CrossRef] [PubMed]
2. European Union Risk Assessment Report. In *1,3,4,6,7,8-Hexahydro-4,6,6,7,8,8-Hexamethylcyclopenta-γ-2-Benzopyran, (1,3,4,6,7,8-Hexahydro-4,6,6,7,8,8-Hexamethylin-Deno[5,6-C]Pyran-Hhcb)*; 1222-05-5; European Chemicals Bureau: Ispra, Italy, 2008.
3. Bester, K. Polycyclic musks in the Ruhr catchment area–transport discharges of waste water, and transformation of HHCB, AHTN and HHCB-lactone. *J. Environ. Monit.* **2005**, *7*, 43–51. [CrossRef] [PubMed]
4. Bester, K. Analysis of musk fragrances in environmental samples. *J. Chromatogr. A* **2009**, *1216*, 470–480. [CrossRef] [PubMed]
5. Peck, A.M.; Hornbuckle, K.C. Synthetic musk fragrances in Lake Michigan. *Environ. Sci. Technol.* **2004**, *28*, 367–372. [CrossRef]
6. Peng, F.-J.; Ying, G.-G.; Pan, C.G.; Seleck, H.; Salvino, D.; Van den Brink, P.J. Bioaccumulation and biotransformation of triclosan and galaxolide in the freshwater oligocaete *Limnodrilus hoffmeisteri* in a water/sediment microcosm. *Environ. Sci Technol.* **2018**, *52*, 8390–8398. [CrossRef]

7. Havranek, I.; Coutris, C.; Norli, H.R.; River, P.-A.; Joner, E.J. Uptake and elimination kinetics of the biocide triclosan and the synthetic musks galaxolide and tonalide in the earthworm *Dendrobaena veneta* when exposed to sewage sludge. *Environ. Toxicol. Chem.* **2017**, *36*, 2068–2073. [CrossRef]
8. Cunha, S.C.; Trabalon, L.; Jacobs, S.; Castro, M.; Fernandez-Tejedor, M.; Granby, K.; Verbeke, W.; Kwadijk, C.; Ferrari, F.; Robbens, J.; et al. UV-filters and musk fragrances in seafood commercialized in Europe Union: Occurrence, risk and exposure assessment. *Environ. Res.* **2018**, *161*, 399–408. [CrossRef]
9. Macherius, A.; Eggen, T.; Lorenz, W.G.; Reemtsma, T.; Winkler, U.; Moeder, M. Uptake of galaxolide, tonalide, and triclosan by carrot, barley, and meadow fescue plants. *J. Agric. Food Chem.* **2012**, *60*, 7785–7791. [CrossRef]
10. Rivier, P.-A.; Havranek, I.; Courtis, C.; Norli, H.R. Joner, E.J. Transfer of organic pollutants from sewage sludge to earthworms and barley under field conditions. *Chemosphere* **2019**, *222*, 954–960. [CrossRef]
11. Sanyal, S.; Amrani, F.; Dallongeviille, A.; Banerjee, S.; Blanchard, O.; Deguen, S.; Costet, N.; Zmirou-Navier, D.; Annesi-Maesano, I. Estimating indoor galaxolide concentrations using predictive models based on objective assessments and data about dwelling characteristics. *Inhal. Toxicol.* **2017**, *29*, 611–619. [CrossRef]
12. Eschke, H.-D. Synthetic musks in different water matrices. In *The Handbook of Environmental Chemistry*; Rimkus, G., Ed.; Springer: Berlin/Heidelberg, Germany, 2004; Volume 3, pp. 17–28.
13. Balk, F.; Ford, R.A. Environmental risk assessment for the polycyclic musks AHTN and HHCB in the EU: I. Fate and Exposure Assessment. *Toxicol. Lett.* **1999**, *111*, 57–79. [CrossRef]
14. Rusconi, M.; Brenna, E.; Polesello, S. Can the ratio galaxolide-lactone: Galaxolide be a good tracer of wastewater in freshwaters? *Integr. Environ. Assess. Manag.* **2017**, *13*, 214–216. [CrossRef]
15. Ilyas, H.; van Hullebush, E.D. Performance comparison of different constructed wetlands for the removal of personal care products. *Environ. Res. Public Health* **2020**, *17*, 3091.
16. Bester, K. Retention characteristics and balance assessment for two polycyclic musk fragrances (HHCB and AHTN) in a typical German sewage treatment plant. *Chemosphere* **2020**, *57*, 863–870. [CrossRef]
17. Simonich, S.L.; Federle, T.W.; Eckhoff, W.S.; Rottiers, A.; Webb, S.; Sabaliunas, D.; de Wolf, W. Removal of fragrance materials during U.S. and European wastewater treatment. *Environ. Sci. Technol.* **2020**, *36*, 2839–2847. [CrossRef]
18. Tasselli, S.; Guzzella, L. Polycyclic musk fragrances (PMFs) in wastewater and activated sludge: Analytical protocol and application to a real case study. *Environ. Sci. Pollut. Res.* **2020**, *27*, 30977–30986. [CrossRef]
19. Cavanagh, J.A.E.; Trought, K.; Mitchell, C.; Northcott, G.; Tremblay, L.A. Assessment of endocrine disruption and oxidative potential of bisphenol A, triclosan, nonylophenol, diethylhexyl phthalate, galaxolide, and carbamazepine, common contaminants of municipal biosolids. *Toxicol. Vitr.* **2018**, *48*, 342–349. [CrossRef]
20. Parolini, M.; Magni, S.; Traversi, I.; Villa, S.; Finizio, A.; Binelli, A. Environmentally relevant concentrations of galaxolide (HHCB) and tonalide (AHTN) induced oxidative and genetic damage in *Dreissena polymorpha*. *J. Hazard. Mater.* **2015**, *285*, 1–10. [CrossRef]
21. Ehiguese, F.O.; Alam Md, R.; Pinado-herrera, M.; Araujo, C.V.M.; Martin-Diaz, M.L. Potential of environmental concentrations of the musks galaxolide and tonalide to induce oxidative stress and genotoxicity in the marine environment. *Mar. Environ. Res.* **2020**, *160*, 105019–105027. [CrossRef]
22. Ding, T.; Li, W.; Cai, M.; Jia, X.; Yang, M.; Yang, B.; Li, J. Algal toxicity, accumulation and metabolic pathway of galaxolide. *J. Hazard. Mater.* **2020**, *384*, 121360–121366. [CrossRef]
23. Martin, C.; Moeder, M.; Daniel, X.; Krauss, G.; Schlosser, D. Biotransformation of the polycyclic musks HHCB and AHTN and metabolite formation by fungi occurring in freshwater environments. *Environ. Sci. Technol.* **2007**, *41*, 5395–5402. [CrossRef] [PubMed]
24. Correia, P.; Cruz, A.; Santos, L.; Alvares, A. Human dermal exposure to galaxolide from personal care products. *Int. J. Cosmet. Sci.* **2013**, *35*, 299–309. [CrossRef]
25. Kannan, K.; Reiner, J.L.; Yun, S.H.; Perrotta, E.E.; Tao, L.; Johnson-Restrepo, B.; Rodan, B.D. Polycyclic musk compounds in higher trophic level aquatic organisms and humans from the United States. *Chemosphere* **2005**, *61*, 693–700. [CrossRef] [PubMed]
26. Yin, J.; Wang, H.; Li, J.; Wu, Y.; Shao, B. Occurrence of synthetic musks in human breast milk samples from twelve provinces in China. *Food Addit. Contam. A* **2016**, *33*, 1219–1227. [CrossRef] [PubMed]
27. Ueno, D.; Moribe, M.; Inoue, K.; Someya, T.; Ryuda, T.; Ichiba, M.; Miyamata, T.; Kunisue, T.; In, H.; Marud, K.; et al. Synthetic musk fragrances in human breast milk and adipose tissue from Japan. *Environ. Res. Asia* **2009**, 247–252.
28. Correia, P.; Cruz, A.; Santos, L.; Alvares, A. Risk of children's dermal exposure to galaxolide through personal care products. *Cosmetics* **2015**, *2*, 93–109. [CrossRef]
29. Bagasra, O.; Golkar, Z.; Garcia, M.; Rice, L.N.; Pace, D.G. Role of perfumes in pathogenesis of autism. *Med. Hypothesis* **2013**, *80*, 795–803. [CrossRef] [PubMed]
30. Sanchez-Prado, L.; Lourido, M.; Lores, M.; Llompart, M.; Garcia-Jares, C.; Cela, R. Study of the photoinduced degradation of polycyclic musk compounds by solid-phase microextraction and gas chromatography/mass spectrometry. *Rapid Commun. Mass Spectrom.* **2004**, *18*, 1186–1192. [CrossRef]
31. Liu, X.; Chena, Z.; Wanga, L.; Wub, Y.; Garoma, T. Degradation of polycyclic musk HHCB in water by O_3, UV, and UV/O_3. *J. Photochem. Photobiol. A* **2012**, *230*, 1–9. [CrossRef]
32. Santiago-Morales, J.; Gomez, M.J.; Herrera, S.; Fernandez-Alba, A.R.; Garcia-Calveo, E.; Rosal, E. Oxidative and photochemical processes for the removal of galaxolide and tonalide from wastewater. *Water Res.* **2012**, *46*, 4435–4447. [CrossRef] [PubMed]

33. Li, W.; Nanaboina, V.; Chen, F.; Korshin, G.V. Removal of polycyclic synthetic musks and antineoplastic drugs in ozonated wastewater: Quantification based on the data of differential spectroscopy. *J. Hazard. Mater.* **2016**, *304*, 242–250. [CrossRef]
34. Calza, P.; Sakkas, V.A.; Medana, C.; Islam, M.A.; Raso, E.; Panagiotou, K.; Albanis, T. Efficiency of TiO_2 photocatalytic degradation of HHCB (1,3,4,6,7,8-hexahydro-4,6,6,7,8,8-hexamethylcyclopenta[γ]-2-benzopyran) in natural aqueous solutions by nested experimental design and mechanism of degradation. *Appl. Catal. B Environ.* **2010**, *99*, 314–320. [CrossRef]
35. Lopez, S.H.; Hernando, D.; Gómez, M.J.; Santiago-Morales, J.; Rosal, R.; Fernández-Alba, A.R. Investigation of Galaxolide Degradation Products Generated under Oxidative and Irradiation Processes by Liquid chromatography/hybrid Quadrupole Time-of-Flight Mass Spectrometry and Comprehensive Two-Dimensional Gas chromatography/Time-of-Flight Mass Spect. *Rapid Commun. Mass Spectrom.* **2013**, *27*, 1237–1250. [CrossRef] [PubMed]
36. Li, Y.; Sun, Y.; Zhang, Q. Theoretical and kinetic properties of OH radical-initiated oxidation of galaxolide in the atmosphere. *J. Phys. Chem. A* **2018**, *122*, 9151–9159. [CrossRef]
37. Wang, X.-H.; Lin, A.Y.-C. Is the phototransformation of pharmaceuticals a natural purification process that decreases ecological and human health risks? *Environ. Pollut.* **2014**, *186*, 203–215. [CrossRef]
38. Kulthong, K.; Srisung, S.; Boonpavanitchakul, K.; Kangwansupamonkon, W.; Maniratanachote, R. Research Determination of silver nanoparticle release from antibacterial fabrics into artificial sweat. *Part. Fibre Toxicol.* **2010**, *1*, 7–8.
39. Vallecillos, L.; Borrull, F.; Pocurull, E. Recent approaches for the determination of synthetic musk fragrances in environmental samples. *Trends Anal. Chem.* **2015**, *72*, 80–92. [CrossRef]
40. Panagiotou, A.N.; Sakkas, V.A.; Albanis, T.A. Application of chemometric assisted dispersive liquid–liquid microextraction to the determination of personal care products in natural waters. *Anal. Chim. Acta* **2009**, *649*, 135–140. [CrossRef]
41. Frisch, M.J.; Trucks, G.W.; Schlegel, H.B.; Scuseria, G.E.; Robb, M.A.; Cheeseman, J.R.; Scalmani, G.; Barone, V.; Petersson, G.A.; Nakatsuji, H. (Eds.) *Gaussian 16*; Revision, C.01; Gaussian, Inc.: Wallingford, CT, USA, 2016.
42. Chemcraft-Graphical Software for Visualization of Quantum Chemistry Computations. Available online: https://www.chemcraftprog.com (accessed on 7 April 2021).
43. Barone, W.; Cossi, M.; Tomasi, J. Geometry optimization of molecular structures in solution by the polarizable continuum model. *J. Comput. Chem.* **1998**, *19*, 404–417. [CrossRef]
44. Zhao, Y.; Truhlar, D.G. The M06 suite of density functionals for main group thermochemistry, thermochemical kinetics, noncovalent interactions, excited states, and transition elements: Two new functionals and systematic testing of four M06-class functionals and 12 other functionals. *Theor. Chem. Acc.* **2008**, *120*, 215–241.
45. Dunning, T.H. Gaussian basis sets for use in correlated molecular calculations. I. The atoms boron through neon and hydrogen. *J. Phys. Chem.* **1989**, *90*, 1007–1023. [CrossRef]
46. Karpińska, J.; Sokół, A.; Kołdys, J.; Ratkiewicz, A. Studies on the Kinetics of Doxazosin Degradation in Simulated Environmental Conditions and Selected Advanced Oxidation Processes. *Water* **2019**, *11*, 1001. [CrossRef]
47. Sadef, Y.; Poulsen, T.G.; Bester, K. Modeling organic micro pollutant degradation kinetics during sewage sludge composting. *Waste Manag.* **2014**, *34*, 2007–2013. [CrossRef]
48. Liu, J.; Zhang, W.; Zhou, Q.; Zhou, Q.; Zhang, Y.; Zhu, L. Polycyclic Musks in the Environment: A Review of Their Concentrations and Distribution, Ecological Effects and Behavior, Current Concerns and Future Prospects. *Crit. Rev. Environ. Sci. Technol.* **2021**, *51*, 323–377. [CrossRef]
49. Gao, S.; Tian, B.; Zeng, X.; Yu, Z. Enantiomeric Analysis of Polycyclic Musks AHTN and HHCB and HHCB-Lactone in Sewage Sludge by Gas chromatography/Tandem Mass Spectrometry. *Rapid Commun. Mass Spectrom.* **2019**, *33*, 607–612. [CrossRef] [PubMed]
50. Biselli, S.; Gatermann, R.; Kallenborn, R.; Sydnes, L.K.; Hühnerfuss, H. Biotic and abiotic transformation pathways of synthetic musks in the aquatic environment. In *Synthetic Musk Fragrances in the Environment. The Handbook of Environmental Chemistry*; Hutzinger, O., Ed.; Springer: Berlin/Heidelberg, Germany, 2004; pp. 189–211.